



Mica, deformation fabrics and the seismic properties of the continental crust

Geoffrey E. Lloyd ^{a,*}, Robert W.H. Butler ^b, Martin Casey ^{a,1}, David Mainprice ^c

^a Institute of Geophysics and Tectonics, School of Earth and Environment, The University of Leeds, Leeds LS2 9JT, UK

^b Geology and Petroleum Geology, School of Geosciences, University of Aberdeen, Meston Building, King's College, Aberdeen AB24 3UE, UK

^c Géosciences Montpellier, CNRS and Université Montpellier 2, 34095 Montpellier, France

ARTICLE INFO

Article history:

Received 19 January 2009

Received in revised form 18 September 2009

Accepted 18 September 2009

Available online 23 October 2009

Editor: R.D. van der Hilst

Keywords:

mica
seismic anisotropy
continental tectonics
S–C fabrics
CPO
EBSD

ABSTRACT

Seismic anisotropy originating within the continental crust is used to determine kinematic flow lines within active mountain belts and is widely attributed to regionally aligned mica. However, naturally deformed micaceous rocks commonly show composite (e.g. S–C) fabrics. It is necessary therefore to understand how both varying mica content and differing intensities of multiple foliations impact on seismic interpretations in terms of deformation fields. An outcrop analogue for granitic mid-crustal deformed zones is used here to calibrate the seismic response against both parameters. Seismic responses are modelled using crystallographic preferred orientations for polymineralic, micaceous granitic gneisses, measured using Electron Back-Scatter Diffraction. The sample results are generalised by modelling the effects of variations in modal composition and the relative importance of deformation fabrics of variable orientation, so-called rock and fabric recipes. The maximum P- and S-anisotropy are calculated at 16.6% and 23.9% for single-foliation gneisses but for mixed (i.e. S–C) foliation gneisses these values reduce to 5.8% and 7.5% respectively. Furthermore, mixtures of multiple foliations generate significant variations in the geometry of the seismic anisotropy. This effect, coupled with the geographical orientation of fabrics in nature, can generate substantial variations in the orientation and magnitude of seismic anisotropy (especially for shear waves) as measured for the continental crust using existing receiver function and teleseismic near-vertical incidence methods. Thus, maps of seismic anisotropy varying with depth in deforming continents need not imply necessarily depth-varying deformation kinematics and tectonic decoupling.

© 2009 Elsevier B.V. All rights reserved.

1. Introduction

Variations in the orientation and strength of seismic anisotropy are used commonly to map deformation in the deep Earth (e.g. Mainprice, 2007). Whilst early researches concentrated on the contribution of crystallographically aligned olivine in the upper mantle as the prime origin for measured seismic anisotropy (e.g. Silver, 1996; Savage, 1999), it is realised now that mineral alignment in the continental crust can contribute also to seismic anisotropy (e.g. Okaya and Christensen, 2002; Vergne et al., 2003; Sherrington et al., 2004; Mainprice, 2007). Consequently, seismic receiver functions and nearby earthquakes are being used increasingly to measure anisotropy in the continental crust (e.g. Ozacar and Zandt, 2004; Champion et al., 2006; Xu et al., 2007).

Acoustic experiments of rock samples indicate that schists exhibit significant P-wave anisotropy and shear wave splitting (e.g. Brocher and Christensen, 1990; Burlini and Fountain, 1993; Godfrey et al., 2000; Cholach and Schmitt, 2006). These experiments have led to a tacit assumption that seismic anisotropy in the continental crust may

reflect regionally aligned micaceous foliation and that its orientation may be used to deduce the geometry of ductile deformation in-situ (e.g. Burlini, 1994; Weiss et al., 1999; Godfrey et al., 2000; Shapiro et al., 2004; Sherrington et al., 2004). Some studies go further, inferring variations in deformation geometry with depth (e.g. Ozacar and Zandt, 2004), while others have mapped zones of apparently enhanced anisotropy that are interpreted as ductile thrust zones (e.g. Schulte-Pelkum et al., 2005). These researches set the agenda for mapping strain in the continental crust and provide ways of relating surface deformation deduced from geodetic data to mantle flow.

The deduction of relationships between geodetic data and mantle flow requires understanding of how bulk seismic properties relate to deformation geometry and kinematics in rocks of the continental crust. For example, whilst pure shear deformations tend to generate rocks with single (parallel) foliation patterns, many simple shear deformations exhibit multiple (non-parallel) foliations (Fig. 1). In particular, in natural simple shear zones, such as ductile faults hosted in granitoids, deformation is commonly characterised by dual, so-called S–C, fabrics developed on scales greater than the grain size, comprising of non-parallel schistosity (S) and shear or cisaillement (C) planes (Berthé et al., 1979; Lister and Snoke, 1984). S-planes are considered to be related to the accumulation of finite strain, whereas C-planes are considered to be related to localised high shear strain. It

* Corresponding author.

E-mail address: g.lloyd@earth.leeds.ac.uk (G.E. Lloyd).

¹ Deceased 2008.

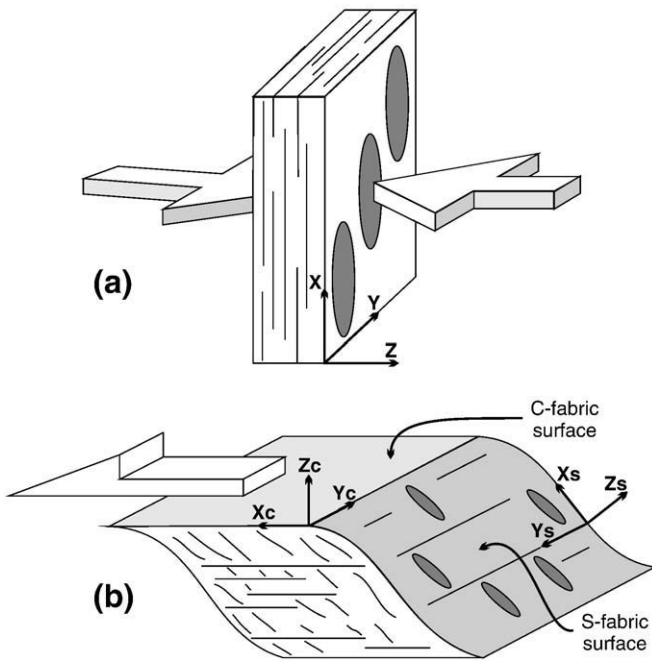


Fig. 1. Kinematic models and tectonic foliations. (a) Pure shear dominant single fabric (note, $X \geq Y \geq Z$). (b) Simple shear dominant dual (S-C) fabrics (note, individual tectonic reference frames for each fabric).

is possible therefore to define distinct tectonic reference frames ($X \geq Y \geq Z$) related to each planar fabric (Fig. 1b). Although S-surfaces are often considered to develop first and to be cross-cut subsequently at high angles by C-planes, simultaneous formation of S-C planes is also possible (e.g. Berthé et al., 1979; Lister and Snoke 1984). The initial high angle between the two sets of planes can decrease with increasing shear strain localised upon the C-planes and eventually both sets of planes may become sub-parallel. The aim here is to show how such multiple (i.e. S-C) deformation fabrics in micaceous rocks, together with varying mica content, combine within a simple kinematic framework to produce significant variations not only in the intensity but also in the orientation of seismic anisotropy.

Almost all of the rock-forming minerals in the continental crust exhibit significant seismic anisotropy as single crystals (Barruol and Mainprice, 1993; Ji et al., 2002). However, for many minerals, including quartz and feldspars, the crystal symmetry creates geometrically complex seismic responses that, with small degrees of misorientation within polycrystalline aggregates, interfere destructively to produce either low anisotropy or near isotropic behaviours. Key exceptions are monoclinic mica and amphibole minerals that commonly align both crystallographic directions and shapes to create a simple seismic anisotropy pattern (e.g. Sherrington et al., 2004 and references therein). Consequently, significant measured seismic anisotropy in the mid continental crust is attributed usually to the crystallographic preferred orientation (CPO) of mica (e.g. Kern and Wenk, 1990; Nishizawa and Yoshino, 2001; Shapiro et al., 2004; Mahan, 2006; Meissner et al., 2006). In the lower continental crust amphibole is likely to be significant also (e.g. Rudnick and Fountain, 1995; Kitamura, 2006; Barberini et al., 2007; Tatham et al., 2008). Other common minerals (e.g. quartz and feldspar) are only expected to contribute constructively to the whole rock seismic anisotropy where mica and/or amphibole are absent. The CPO-based approach excludes open fractures (e.g. see Crampin and Chastin, 2003), grain-scale effects (e.g. Hall et al., 2008), sedimentary layering (e.g. Valcke et al., 2006) and other microstructural parameters (e.g. Wendt et al., 2003) that might contribute also to seismic anisotropy in certain circumstances.

To investigate the kinematic significance of seismic anisotropy measurements in the middle continental crust, a sample exhibiting mica S-C fabrics is used here. The sample is from the Nanga Parbat massif, NW Pakistan, where there is a good kinematic framework (Butler et al., 2002) and mid-crustal materials have been exhumed rapidly from the depths where they were actively deforming (e.g. Zeitler et al., 1993, 2001). In addition, acoustic anisotropy has been measured in rock samples from Nanga Parbat by Meltzer and Christensen (2001). They report effective seismic anisotropies of up to 12% for compression waves and 21% for shear waves transmitted through Nanga Parbat gneisses and attribute these values to strongly aligned biotite. The current paper relates seismic properties explicitly to deformation structures on the scale of polycrystalline aggregates. These results are used then to produce a generalised model for the seismic response of deformed micaceous continental crust linked to mica content and deformation fabrics.

2. Constructing seismic properties

The procedure for using microstructural data to predict the seismic response of deformed polycrystalline aggregates followed in this paper is similar to that employed in a companion contribution that studies the seismic properties of basic continental crust and the role of amphibole (Tatham et al., 2008). However, the approach was originally developed to calibrate the seismic properties of the upper mantle by using peridotite xenoliths (Crosson and Lin, 1971; Mainprice and Silver, 1993; Ben Ismail and Mainprice, 1998). For these mantle rocks, the orientation of each crystal of olivine within the aggregate is measured. This is possible now, both accurately and efficiently via automation, for thousands of grains in polycrystalline samples using Electron Back-scattered Diffraction (EBSD). The elastic properties for single crystals can then be summed over the aggregate to determine the seismic response for the bulk rock, thereby linking the deformation fabrics (e.g. kinematic lineation and foliation) to the seismic response (e.g. Mainprice, 1990; Mainprice and Humbert, 1994). Thus, seismic anisotropy measurements for the mantle and crust can be interpreted in terms of deformation flow fields (e.g. Mainprice and Nicolas, 1989; Babuska and Cara, 1991).

The methodology for monomineralic olivine rocks has been modified for the continental crust by using appropriate elastic properties for crustal minerals, combined in proportions appropriate to those measured in polymineralic aggregates (e.g. Mainprice and Humbert, 1994). Such an approach has advantages because the different components of the bulk mineralogy can be varied to investigate not only the relative contributions of individual mineral phases (the 'rock recipe') but also differently oriented fabric elements (e.g. S-C foliations, the 'fabric recipe'). Both of these approaches are considered here, with the seismic properties calculated for each recipe according to standard procedure using the following elastic constants: quartz (McSkimin et al., 1965); plagioclase (Aleksandrov et al., 1974); orthoclase (Aleksandrov et al., 1974); biotite (Aleksandrov and Ryzhova, 1961); and muscovite (Vaughan and Guggenheim, 1986).

3. Sample description

The sample used in this study is an orthogneiss from the Nanga Parbat Massif, Western Himalaya. These gneisses are derived largely from a granodioritic protolith composed of feldspar, quartz and biotite, with subordinate muscovite (Fig. 2). Overall, this composition is a good analogue for much of the Earth's middle continental crust (e.g. Barruol and Mainprice, 1993; Rudnick and Fountain, 1995). In deformed state some of the feldspars form distinctive megacrysts (augen) that provide strain markers and rigid bodies that aid definition of the deformation state (Butler et al., 2002). Using this observation, two end-member foliation types can be described (Butler et al., 2002): 1. a subvertical stretching foliation produced by near co-

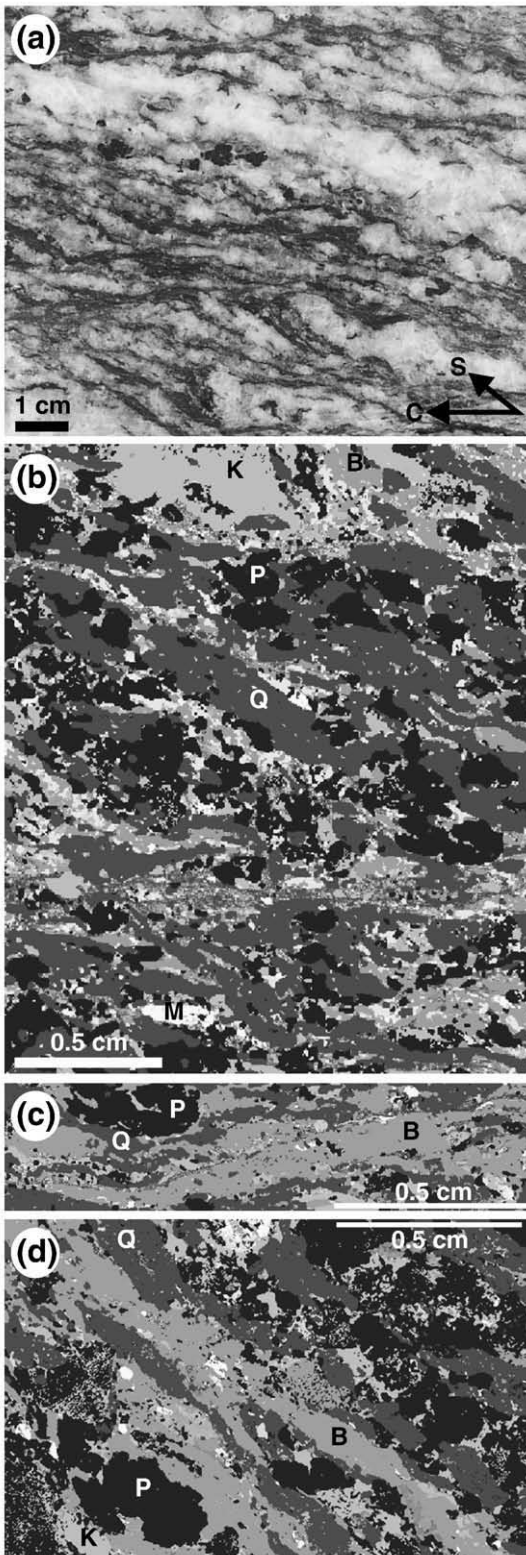


Fig. 2. Sample of Nanga Parbat gneisses used in EBSD analysis and rock and fabric modelling. All images are XZ planes (X horizontal, Z vertical). (a) Hand-specimen from which the EBSD sample was cut; note C- and S- fabrics. (b)–(d) Grey-scale coded EBSD mineral phase images (B, biotite mica; K, orthoclase feldspar; M, muscovite mica; P, plagioclase feldspar; Q, quartz). (b) Whole sample. (c) C-fabric sample (note horizontal biotite). (d) S-fabric sample (note inclined biotite).

axial sub-horizontal shortening; and 2. a gently SSE-dipping foliation formed by strongly localised, top-NNW simple shear (thrusting). These foliations interact to form a tract of gneisses that exhibit both

vertical stretching and shearing, manifest as cm-scale domains that collectively define S–C fabrics (in the sense of Lister and Snoke, 1984).

A single, representative (in terms of bulk mineralogy and deformation state) sample of Nanga Parbat gneiss from field site B1 of Butler et al. (2002) with well-developed S–C fabrics was selected for detailed petrographic analysis and seismic property determination (Fig. 2). The geographical orientation of the sample was recorded at the time of sampling so that the microstructural and seismic properties could be reported and analysed in their in-situ geometry. The sample is typical of Nanga Parbat massif gneisses, containing quartz, plagioclase and orthoclase feldspars, together with abundant biotite and muscovite micas that contribute to the domains of strong S and C foliations. The domainal nature of the deformation allows the two distinct fabric elements (i.e. S and C) to be isolated and measured separately. The role of the two fabrics in contributing to the bulk lattice preferred orientation and hence the seismic response of the gneisses as a whole can be investigated then by re-combining them in varying proportions. This constitutes the ‘fabric recipe’.

The sample was oriented kinematically with X (axis of maximum tectonic elongation) horizontal, Z (direction of maximum tectonic contraction) vertical and Y (remaining Cartesian direction) normal to the plane of section. Such XZ sections contain usually the most significant kinematic shear criteria, especially for plane strain deformations. Both the S- and C-fabrics are defined predominantly by micas, especially biotite, although quartz is elongate typically parallel to both foliations and the shape of the orthoclase augen reflects the different kinematic components. In contrast, plagioclase grains are commonly equant. The C-fabric is parallel to the macroscopic XY plane but the S-fabric is considerably steeper, although somewhat variable in inclination within the sample (Fig. 2). The two fabrics form distinctive and separate elements in the microstructure and can be analysed therefore individually via EBSD (see Supplementary Information for analytical details).

Three specific EBSD analyses were performed (Fig. 2): (1) whole sample; (2) a region comprising the C-type fabric; and (3) a region comprising the S-type fabric. The modal proportions for each EBSD analysis are given in Table 1. The S- and C-fabric analyses are not expected to yield similar modal proportions to the whole sample analysis as these regions were targeted specifically for their biotite-rich foliations.

The individual mineral CPO in each analysis was determined via EBSD, from which the sample seismic properties were derived via standard procedure (e.g. Barruol and Mainprice, 1993; Mainprice and Humbert, 1994; Lloyd and Kendall, 2005; Tatham et al., 2008). To assess the role of biotite in determining seismic properties, the modal content of biotite in the whole sample analysis was varied between 0 and 100% whilst the other phases were varied according to their as-measured proportions (see Table 1a) to provide a range of rock recipes. To assess the role of S–C fabrics in determining seismic properties, the biotite contents of the C-fabric and S-fabric samples (Table 1b, c) were combined into a single dataset within which the different fabric elements could be distinguished and hence varied in their relative proportions between 0 and 100% (i.e. fabric recipes). Furthermore, it is possible to combine the results of the rock and fabric

Table 1

EBSD-derived modal proportions (%) of minerals in the Nanga Parbat gneiss sample. The full data are presented as Supplementary Information.

Phase	(a) Whole sample	(b) C-type fabric	(c) S-type fabric
Quartz	35.2	32.3	25.1
Plagioclase	33.0	21.4	40.9
Orthoclase	11.9	9.2	10.8
Biotite	10.3	37.1	23.2
Muscovite	9.6	–	–

recipe analyses to assess the overall control of mineral and fabric contents on seismic properties.

4. Results

The conventional displays for CPO and seismic properties are in a reference frame of the strain geometry (i.e. XYZ), with foliation (XY plane) vertical and E–W, and lineation E–W and horizontal. This convention allows the microstructure to be directly linked to the deformation kinematics, assuming that both the foliation and lineation track the finite strain, especially when the CPO is asymmetric. However, it is more appropriate to consider the seismic properties in terms of geographic coordinates as this provides a direct link to real seismic survey observations. Here CPO is presented initially therefore in XYZ-coordinates (Fig. 3a) but are subsequently rotated into geographic coordinates (Fig. 3b). The outcrop for the sample contains the regional C-foliation (i.e. XY-plane and normal-Z) with ~ENE–WSW strike and shallow ~SSE dip together with the regional stretching lineation (i.e. X) with shallow plunge towards ~SSE azimuth. The regional foliation normal (i.e. Z) plunges steeply towards the ~NNW, whilst the intermediate axis (Y) is oriented approximately horizontally parallel to the ~ENE–WSW strike of this foliation. Knowledge of these orientations permits the rotation of measured CPO into the geographic orientation of the samples.

The approach adopted here, particularly when combined with rock and fabric modelling, generates a significant amount of output in the form of stereographic projections. Much of this is available in this paper's Supplementary Information. The results for the actual sample composition (Table 1a) and C:S fabric ratio recipes for 20% modal biotite are presented here (Fig. 3). The latter represents the total mica composition of the rock sample but as the C- and S-fabric samples contain only biotite the muscovite component is considered as biotite to simplify analysis. To emphasise further the significant role of biotite in controlling seismic properties, results are presented also assuming 100% modal biotite (i.e. all other phases absent). The individual CPO diagrams and seismic models for all the constituent minerals other than biotite are reported in the Supplementary Information.

4.1. CPO

Biotite exhibits strong but variable CPO patterns. In the whole rock (Fig. 3a), maxima in *a* and *c* are inclined to X and Z respectively, with *a* and *b* forming a girdle inclined to XY. In the C-fabric (Fig. 3a), *a* and *b* form a girdle distribution parallel to XY, with the maximum in *c* normal to this (i.e. parallel to Z), the maximum in *a* intermediate between X and Y, and the maximum in *b* sub-parallel to X. In the S-fabric (Fig. 3a), *a* and *b* form a girdle distribution inclined at ~45° to XY, steeper than that observed for the whole sample, with the maxima in *a* and *c* intermediate between XZ and the maximum in *b* intermediate between Y and Z. These relationships suggest that the 'foliation' indicated by the biotite CPO in the whole sample is an average of two individual foliations defined by the (shallower) C- and (steeper) S-fabrics.

4.2. Seismic properties

The particular seismic properties derived here are the compressional wave velocity (Vp km/s) and anisotropy (AVp %), shear wave splitting anisotropy (AVs %) and polarisation (or birefringence) of the fastest shear wave (Vs1P). It should be noted that AVp has no azimuthal significance and refers to variations in P-wave velocities over all directions in contrast to AVs, which refers to an individual ray path. Results for fast and slow shear wave velocities (Vs1, Vs2 km/s) and anisotropies (AVs1, AVs2 %) and difference in shear wave splitting (dVs km/s) are presented as Supplementary Information. To enable direct comparison with the CPO, seismic property distributions are

represented initially in kinematic coordinates. Table 2 lists their maximum and minimum values for the whole and two sub-fabric samples.

As expected, the seismic property distributions reflect the biotite CPO in the three analyses (Fig. 3a). In general, the other mineral phases act simply to dilute the impact of the biotite. In particular, the largest Vp and AVs values mimic the orientation of the biotite foliation, whilst the minimum values are close to the foliation normal. However, the absolute maxima in Vp and AVs are more varied in orientation, both within and between the three analyses. This behaviour reflects the local influence of the C- and S-fabrics and their averaging over the whole sample. In terms of the regional XYZ coordinate system, both the whole sample and the C-fabric have Vp-max sub-parallel to Y but for the S-fabric it is oriented between X and Z (Fig. 3a). In contrast, the maxima in AVs are sub-parallel to Y for the whole sample and the S-fabric but sub-parallel to X for the C-fabric. The polarisation of the fastest shear wave is constrained to be parallel to the dominant foliation in all three samples.

The full impact of biotite on the seismic properties of the three samples is emphasised by considering that each sample consists of 100% biotite (Fig. 3a). There is little difference in the geometry of the seismic results for rocks with 20% or 100% biotite, although of course the absolute values of velocity and anisotropy do vary.

4.3. Geographic coordinates

The kinematic CPO and seismic property results (Fig. 3a) are rotated in Fig. 3b into geographic coordinates to assess their seismological and geodynamic significance. Although the geographic CPO is unusual in appearance structurally, using this reference frame places it in a regional context that can guide better interpretations of seismic data.

Biotite defines the foliation in each sample and both the orientation of the regional foliation and the difference in orientation between the C- and S-fabrics are clear. The fact that the orientations of the regional and C-fabric foliations are similar, whilst the S-fabric foliation is much steeper, suggests that the C-fabric dominates over the S-fabric in the sample considered (see Fig. 3b). However, it is the detail of these patterns, and in particular the positions of the maxima and minima, that are of prime significance seismically.

Whilst the minima in both Vp and AVs define the pole to the various foliations, their maxima are oriented closer to the ~ESE–WSW strike (i.e. Y) rather than the shallow ~SSE plunging stretching lineation (i.e. X). If representative for these types of lithologies, this result contrasts with the general assumption that Vp and AVs maxima align parallel to the direction of maximum kinematic elongation.

4.4. Rock and fabric recipe modelling

The specimen considered here (Fig. 2) represents a sample from a population defined by two simple variables, namely mineral modal content and relative proportion of C- and S-fabrics. The intensity of development of CPO (i.e. a proxy for strain magnitude) can be ignored as the gneisses are all highly deformed and it is assumed therefore that the individual mineral CPO have all reached steady-state and are typical for these rocks. The results of CPO analysis for the whole sample and the two sub-fabric areas (Fig. 3) indicate that it is biotite that controls the seismic properties of the whole rock. Supplementary Information is provided to show in detail how varying biotite content from 0 to 100% whilst the modal content of the other minerals is varied according to their proportions in the actual sample (i.e. rock recipe modelling, see Table 3a) affects the seismic properties.

Having recognised that biotite content is the controlling compositional variable, the potential impact of the two biotite sub-fabrics now needs to be considered. Thus, fabric recipes (Table 3b) have been used, whereby the relative proportions of biotite in each C- and S-fabric sub-

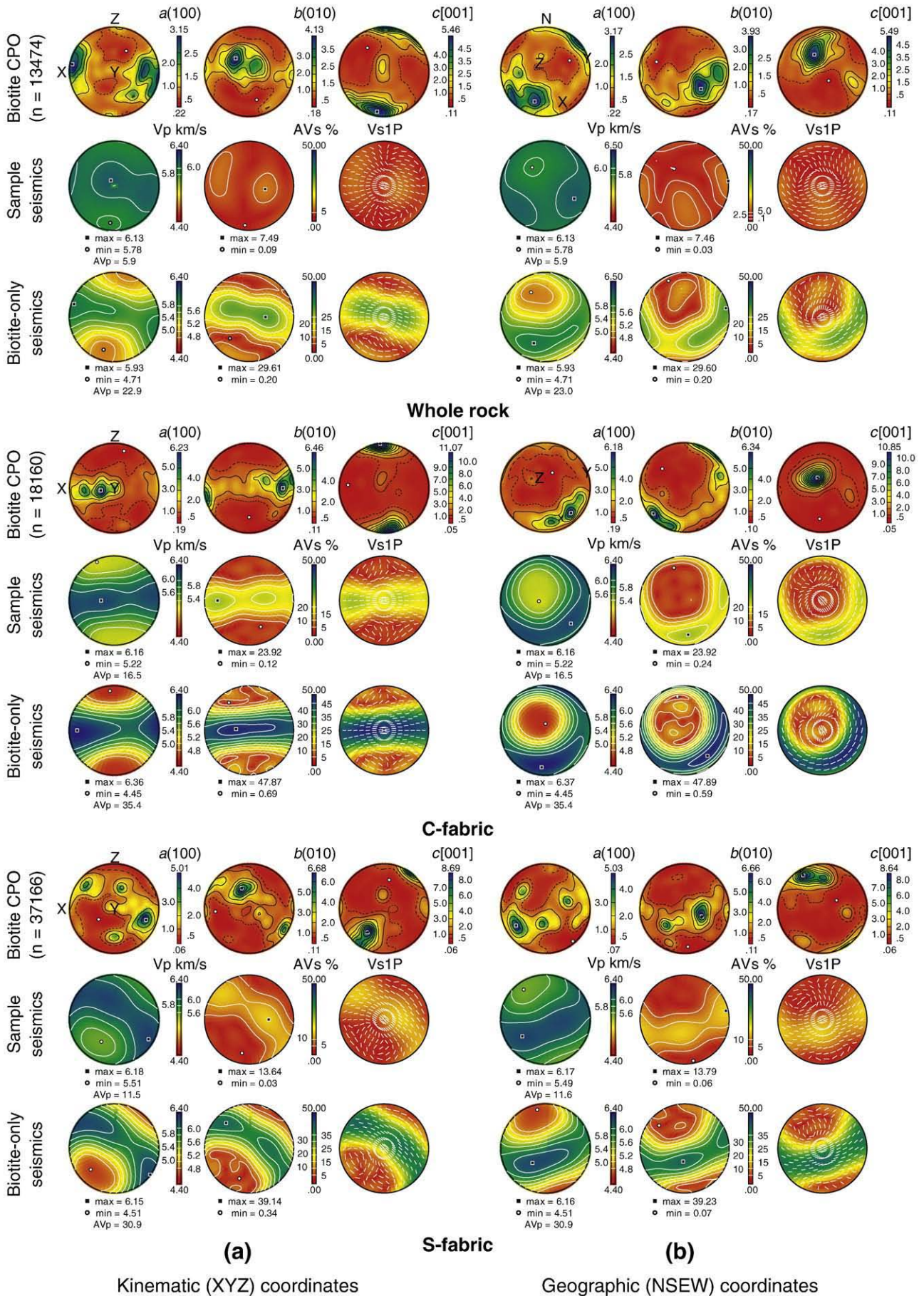


Table 2
Summary of EBSD-derived seismic properties for typical Nanga Parbat gneisses.

Seismic property	Whole sample	C-fabric	S-fabric
Vp km/s	5.8–6.1	5.3–6.2	5.5–6.2
AVp %	5.9	16.6	11.6
AVs %	7.5	23.9	13.7

Table 3
Basic data used in rock and fabric recipe modelling. The actual sample is represented by 20% total mica content (Fig. 4) while results from this array are presented as Supplementary Information. (a) Rock recipes. (b) Fabric recipes.

(a)						
Mica %	0	20	40	60	80	100
Biotite	0	20	40	60	80	100
Plagioclase	41	33	25	16	8	0
Orthoclase	15	12	9	6	3	0
Quartz	44	35	26	18	0	0
SUM	100	100	100	100	100	100
(b)						
Biotite C:S %	0	20	40	60	80	100
100:0	0	20:0	40:0	60:0	80:0	100:0
75:25	0	15:5	30:10	45:15	60:20	75:25
50:50	0	10:10	20:20	30:30	40:40	50:50
25:75	0	5:15	10:30	15:45	20:60	25:75
0:100	0	0:20	0:40	0:60	0:80	0:100

type are varied proportionally between 0 and 100% within the limits provided by the rock recipe modal compositions (Table 3a). The results for the actual sample composition, modelled with a 20% mica fraction that is entirely biotite, are reported in Table 3. The full range of fabric recipe modelling results is provided as Supplementary Information.

Whilst the seismic properties for the 20% biotite fabric recipe are similar, they reflect also a migration in orientation of the C- and S-fabrics as their relative proportions change (Fig. 4; see also Fig. 1b). Thus, for C-fabric dominated rocks, the foliation is relatively shallow, ~SSE-dipping and defines a girdle of similar Vp velocities within which the absolute maximum is sub-parallel to the ~WSW–ENE strike. In contrast, the foliation for S-fabric dominated rocks is steeper but defines still a girdle of high Vp values within which the absolute maximum is again sub-parallel to the ~WSW–ENE strike. In both cases, clear maxima in AVs are defined that plunge sub-parallel to the dip directions of these foliations. As the relative proportions of C- and S-fabrics vary between the two end-member configurations, the girdle in Vp becomes less-well defined and a clear maximum develops parallel to the ~WSW–ENE foliation strike. For AVs, discrete high value concentrations develop within the foliation strike-parallel girdle such that the end-member single maxima disappear (Fig. 4). For approximately equal contributions of C- and S-fabrics, a maximum in AVs is defined sub-parallel to the ~WSW–ENE foliation strike. In terms of vertically propagating (i.e. teleseismic) rays, there is a progressive change from relatively low Vs1 velocities polarised ~NW–SE (i.e. normal to foliation) for 100% C-fabric rocks, to relatively high Vs1 velocities polarised sub-parallel to the foliation (i.e. ~SW–NE) for 100% S-fabric rocks (Fig. 4).

5. Discussion

The modelled seismic response of the sample of Nanga Parbat gneiss shows that the geometry and intensity of anisotropy relates both to the bulk biotite content and the relative proportions of S and C foliations.

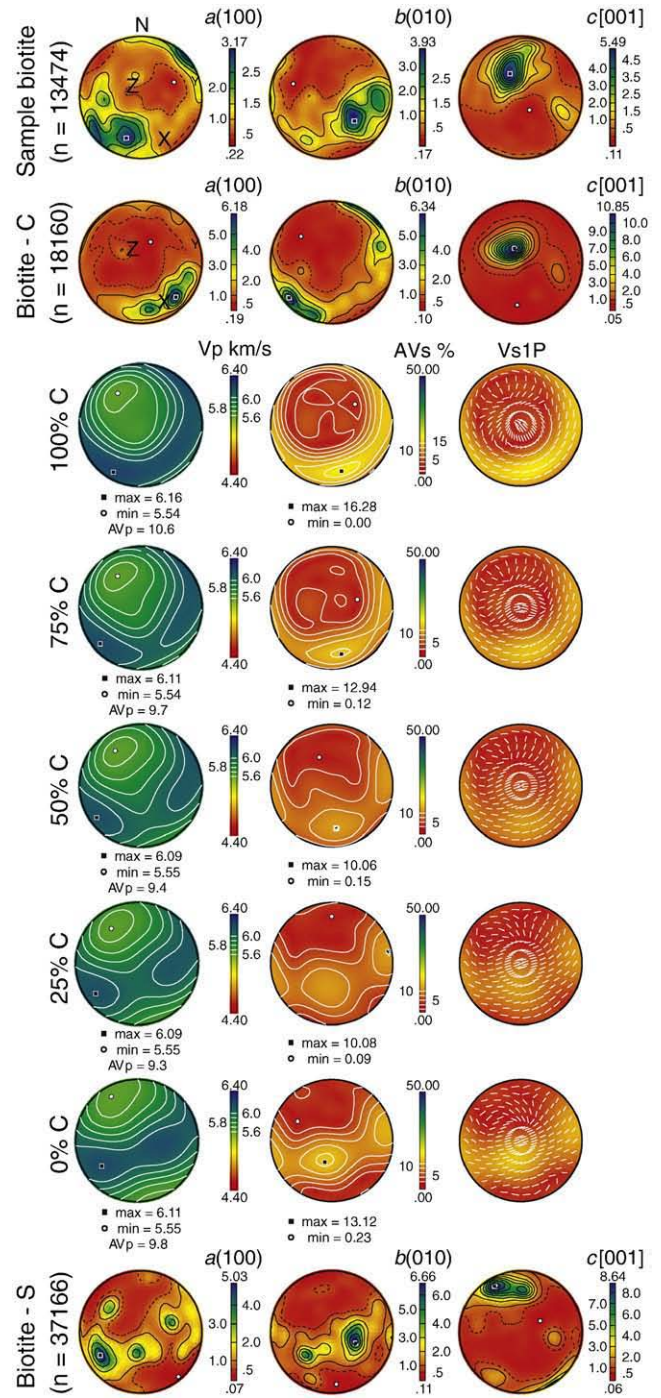
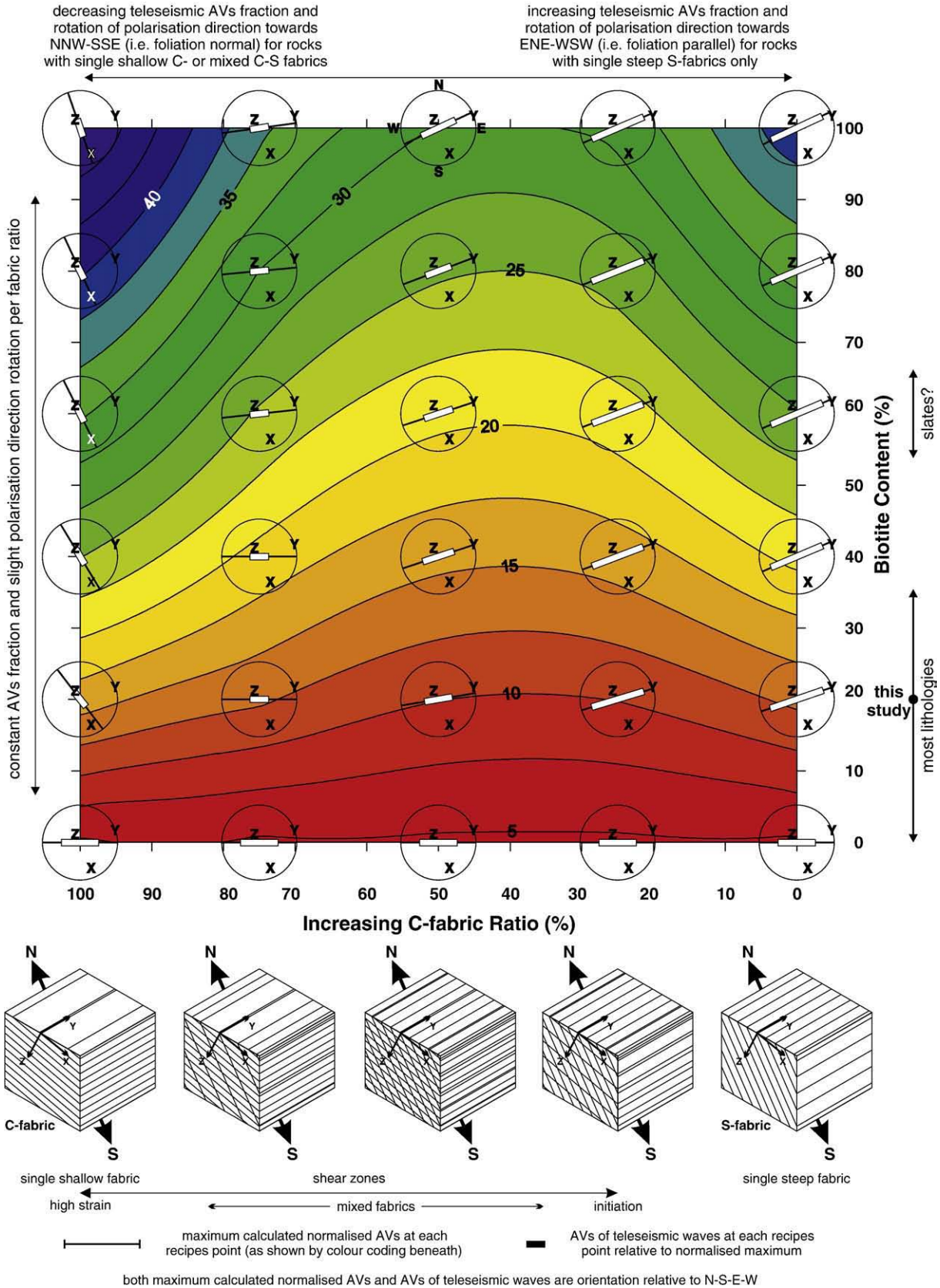


Fig. 4. Fabric ratio recipe results for the actual rock composition, assuming biotite comprises the whole mica modal content of 20%. The top two rows are the whole sample and C-fabric sample CPO; the bottom row is the S-fabric sample CPO. The other rows represent the Vp, AVs and polarisation (Vs1P) seismic properties for the whole rock as the S–C fabric ratio is progressively varied (as indicated left) between the absolute end members. All plots are lower hemisphere, geographic coordinates. All CPO are contoured in terms of multiples of the uniform distribution (m.u.d.). Seismic properties are contoured as indicated (note, the same contour range has been used for each property to facilitate comparison). The full range of fabric ratio recipe modelling results is provided in Supplementary Information.

Fig. 3. EBSD-derived biotite CPO and seismic properties in (a) kinematic (XYZ) and (b) geographic (NSEW) coordinates, assuming as-measured mineral modal proportions, where biotite comprises 20% mica content (see Supplementary Information for CPO of other minerals). Also shown for comparison are the seismic properties assuming 100% biotite composition. All stereographic projections are lower hemisphere. All CPO are contoured in terms of multiples of the uniform distribution (m.u.d.). Seismic properties are contoured as indicated (note, the same contour range has been used for each property to facilitate comparison).

These two controls have been investigated using rock and fabric recipes, reproduced in full within the Supplementary Information. Here, discussion is served by considering shear wave behaviour alone.

Fig. 5 shows how both the intensity and geometry of seismic anisotropy relate to biotite content and relative proportions of S and C fabrics (see also Fig. 1b). The maximum magnitude of AVs (i.e. the



amount of shear wave splitting for a unit thickness of gneiss through which the shear waves are propagating) increases with biotite content and towards the end members of both fabric types. The effect of composite foliations (i.e. S–C fabric as opposed to 100% S or 100% C) is to weaken the magnitude of AVs. Thus, tracts of single schistosity generate stronger maximum anisotropy than rocks with multiple schistositities. This result confirms the direct acoustic measurements of similar Nanga Parbat gneisses with different internal foliation structures reported by Meltzer and Christensen (2001; see also Okaya and Christensen, 2002, for the general impact of mica foliation on seismic wave propagation).

Many seismic experiments either are not configured or the results are not reported to define maximum values of shear wave anisotropy for the crust. Some specially designed near-vertical and wide-angle seismic experiments put constraints on crustal anisotropy (e.g. Meissner et al., 2002; Readman et al., 2009). Recently, near-vertical teleseismic P-wave arrivals, which produce converted S-waves at the Moho and crustal interfaces, have been used to detect azimuthal anisotropy at various depths in the crust using receiver function analysis (e.g. Vergne et al., 2003; Ozacar and Zandt, 2004; Sherrington et al., 2004; Schulte-Pelkum et al., 2005). Anisotropy is illustrated in terms of the orientation of maximum polarisation in the plane of the Earth's surface, and the intensity of this anisotropy in terms of split times for the fast and slow shear waves. The model results from the sample considered in this contribution are presented in similar fashion, overlain on the matrix of biotite content vs. S–C fabric ratio, in geographical coordinates (Fig. 5). The actual regional orientations of S (strike, dip) and C (strike, dip) foliations are explicitly included. Not only does the intensity of the seismic anisotropy deviate significantly from the maximum values, but there is a variation in the orientation of maximum polarisation too. This orientation variation is not a reflection of different kinematics (specifically, shortening directions) but reflects the differing distributions of mica in the rock (namely, the varying proportions of S and C fabrics).

The results of the modelling, as summarised for AVs in Fig. 5, raise issues in the interpretation of seismic anisotropy results. For example, P and S wave anisotropy derived from seismic receiver functions is interpreted by Ozacar and Zandt (2004) as being due to depth variations in the intensity and orientation of seismic anisotropy in the crust, which they explain via a three-layered structural model. However, these authors assume that the seismic properties relate to a single, presumed mica-defined foliation within each layer. An alternative explanation, yet to be tested, is that the deformation kinematics do not vary with depth. Rather, there is depth-dependent partitioning of the deformation into composite, multiple foliations and/or differing mineralogy (i.e. mica, or even amphibole, content), which need not require the intra-crustal decoupling of deformation. Similarly, azimuthal variations in SKS anisotropy obtained from the INDEPTH III seismic profile (e.g. Huang et al., 2000) need not relate simply to variations in flow patterns in the lithosphere but indicate a significant crustal contribution to the overall anisotropy. Godfrey et al. (2000) have suggested that steeply dipping schists in the crust could contribute up to 45% of the SKS anisotropy, whilst Bank and Bostock (2003) found lower crustal S wave anisotropy of 3–7% in Archean and Proterozoic regions of the Canadian shield using forward modelling of P to SV and SH conversions.

Schulte-Pelkum et al. (2005) used teleseismic receiver functions to define a narrow tract in the mid-crust beneath the central Himalaya with AVp of ~20%. These authors suggest that this inclined zone, which projects up to the active Himalayan thrust front, reflects

aligned mica foliations within a ductile shear zone. However, the slow wave direction is gently inclined in the direction of thrusting, implying that the foliation within the shear zone is generally steep. Both Schulte-Pelkum et al. (2005) and Mahan (2006) suggest that this is due to a strong S–C fabric (e.g. Fig. 1b). The modelling results presented here require shear zone rocks with biotite contents in excess of 50% and equally proportioned S–C fabrics to achieve the observed 20% in AVp. Such biotite contents are more consistent with slates than normal felsic rocks. Furthermore, given the probable dimensions and shear strain of this ductile shear zone (e.g. Mahan, 2006), any steep S-fabric that might have developed initially at lower shear strains would have rotated in to sub-parallelism with the dominant C-fabric oriented approximately parallel to the shallowly dipping shear zone margins. Thus, Schulte-Pelkum et al.'s (2005) results are more consistent with a single, steep foliation (e.g. as found in slate belts). A future test therefore would be to use shear wave anisotropy to look for the patterns of polarisation derived via rock and fabric recipe modelling of the sample of Nanga Parbat gneisses described here.

6. Conclusions

The results obtained in this study suggest that if the middle continental crust is dominated by felsic/granitic compositions, then mica is the dominant contributor to the generation of seismic anisotropy. This study confirms the empirical results of Meltzer and Christensen (2001) that rocks with single foliations show stronger absolute seismic anisotropy than those with multiple foliations. For example, the sample considered here, with ~20% biotite by volume, exhibits a maximum of ~16% compressional wave anisotropy (AVp) for single foliation (C-plane only) domains compared with a value of ~6% for equi-proportional S- and C-fabric domains. The shear wave splitting anisotropy (AVs) is ~24% for single C-domains but only ~7% for composite (S–C) fabrics. However, the effect of composite fabrics is not merely to dilute the maximum values of seismic anisotropy, it influences also the geometry. Shear wave anisotropy is particularly sensitive to this effect and can generate orientations of the maxima in predicted polarisation direction that diverge substantially from the trajectories of principal strain axes or kinematic flow lines. Measurements of seismic anisotropy in nature necessarily integrate the effects of the concentration of mica in the rock, together with the organisation of mica into single or multiple foliations and the orientation of these foliations relative to the seismic ray paths. Thus, variations in the orientations of fast polarisation directions for shear waves deduced for different levels in the continental lithosphere need not imply that deformation decouples with depth.

Acknowledgements

Fieldwork in Pakistan was funded by the Royal Society. C. Bond, R. Jones, P. McDade and Z. Shipton are thanked for discussions in the field, together with the University of Peshawar for logistical support and advice. The Leeds EBSD system was funded by UK NERC Grant GR9/3223 (GEL, MC). This research was first presented at the Fall Meeting of the American Geophysical Union in 2005; we thank participants for useful discussions. We thank also the Journal's referees, Luigi Burlini, Mike Kendall and anonymous, and editor, Rob van der Hilst, for their constructive reviews and assistance that together helped to improve the final version.

Fig. 5. Summary and implications of rock and fabric recipes modelling for seismic anisotropy interpretation (AVs). Background colour-coding reflects the predicted AVs values. Circles define the geographic coordinate system and regional orientation of the principal tectonic axes (XYZ). Thin diameter lines indicate the orientation of the fast polarisation direction (FPD) for vertical (teleseismic) waves, with the length representing the maximum AVs value predicted at that point, as defined by the colour contour beneath. Length of the thicker, white-boxed line represents the proportion of the maximum AVs recognised at each modelling point by teleseismic waves. Block diagrams are schematic representations of rocks with different S–C fabric ratios (see horizontal axis), oriented according to the sample used in the modelling. The blocks can be considered also in terms of progressive deformation (e.g. shear zone evolution) during which S-type fabrics initiate at high angles to C-type fabrics and progressively rotate towards them with increasing strain, eventually contributing to the total C-fabric component rather than defining distinct multiple S–C fabrics.

Appendix A. Supplementary data

Supplementary data associated with this article can be found, in the online version, at doi: [10.1016/j.epsl.2009.09.035](https://doi.org/10.1016/j.epsl.2009.09.035).

References

- Aleksandrov, K.S., Ryzhova, T.V., 1961. The elastic properties of rock-forming minerals, I: pyroxenes and amphiboles. *Izv. Acad. Sci. USSR, Geophys. Ser.* 9, 1339–1344 (in Russian).
- Aleksandrov, K.S., Alchikov, V.V., Belikov, B.P., Zaslavskii, B.I., Krupnyi, A.I., 1974. Velocities of elastic waves in minerals at atmospheric pressure and increasing of precision of elastic constants by means of EVM. *Izv. Acad. Sci. USSR, Geophys. Ser.* 10, 15–24 (in Russian).
- Babuska, V., Cara, M., 1991. *Seismic Anisotropy in the Earth*. Kluwer Academic, Dordrecht.
- Bank, C.-G., Bostock, M.G., 2003. Linearized inverse scattering of teleseismic waves for anisotropic crust and mantle structure: 2. Numerical examples and application to data from Canadian stations. *J. Geophys. Res.* 108 (B5), 2259. doi:10.1029/2002JB001951.
- Barberini, V., Burlini, L., Zappone, A., 2007. Elastic properties, fabric and seismic anisotropy of amphibolites and their contribution to the lower crust reflectivity. *Tectonophysics* 445, 227–244.
- Ben Ismail, W., Mainprice, D., 1998. An olivine fabric database: an overview of upper mantle fabrics and seismic anisotropy. *Tectonophysics* 296, 145–157.
- Barruol, G., Mainprice, D., 1993. 3-D seismic velocities calculated from lattice-preferred orientation and reflectivity of a lower crustal section: examples of the Val Sesia section (Ivrea zone, northern Italy). *Geophys. J. Int.* 115, 1169–1188.
- Berthé, D., Choukroune, P., Gapais, D., 1979. Orientations préférentielles du quartz et orthogneissification progressive en régime cisailant: l'exemple du cisaillement sud-armoricain. *Bull. Min.* 102, 265–272.
- Brocher, T.M., Christensen, N.I., 1990. Seismic anisotropy due to preferred mineral orientations observed in shallow crustal rocks in southern Alaska. *Geology* 18, 737–740.
- Burlini, L., 1994. A model for the calculation of the seismic properties of geologic units. *Surv. Geophys.* 15, 593–617.
- Burlini, L., Fountain, D.M., 1993. Seismic anisotropy of metapelites from the Ivrea-Verbano zone and Serie dei Laghi (northern Italy). *Phys. Earth Planet. Inter.* 78, 301–317.
- Butler, R.W.H., Casey, M., Lloyd, G.E., Bond, C.E., McDade, P., Shipton, Z., Jones, R., 2002. Vertical stretching and crustal thickening at Nanga Parbat, Pakistan Himalaya: a model for distributed continental deformation during mountain building. *Tectonics* 21. doi:10.1029/2001TC901022.
- Champion, M.E., White, N.J., Jones, S.M., Priestley, K.F., 2006. Crustal velocity structure of the British Isles: a comparison of receiver functions and wide-angle seismic data. *Geophys. J. Int.* 166, 795–813.
- Cholach, P.Y., Schmitt, D.R., 2006. Intrinsic elasticity of a textured transversely isotropic muscovite aggregate: comparisons to the seismic anisotropy of schists and shales. *J. Geophys. Res.* 111, B09410. doi:10.1029/2005JB004158.
- Crampin, S., Chastin, S., 2003. A review of shear wave splitting in the crack-critical crust. *Geophys. J. Int.* 155, 221–240.
- Crosson, R.S., Lin, J.W., 1971. Voigt and Reuss prediction of anisotropic elasticity of dunite. *J. Geophys. Res.* 76, 570–578.
- Godfrey, N.J., Christensen, N.I., Okaya, D.A., 2000. Anisotropy of schists: contribution of crustal anisotropy to active source seismic experiments and shear wave splitting observations. *J. Geophys. Res.* 105, 27991–28007.
- Hall, S.A., Kendall, J.-M., Maddock, J., Fisher, Q., 2008. Crack density tensor inversion for analysis of changes in rock frame architecture. *Geophys. J. Int.* 173, 577–592.
- Huang, W.C., Ni, J.F., Tilmann, F., Nelson, D., Guo, J.R., Zhao, W.J., Mechie, J., Kind, R., Saul, J., Rapine, R., Hearn, T.M., 2000. Seismic polarization anisotropy beneath the central Tibetan Plateau. *J. Geophys. Res.* 105, 27979–27989.
- Ji, S., Wang, Q., Xia, B., 2002. *Handbook of Seismic Properties of Minerals, Rocks and Ores*. Polytechnic International Press, Canada.
- Kern, H., Wenk, H.-R., 1990. Fabric-related velocity anisotropy and shear wave splitting in rocks from Santa Rosa Mylonite Zone, California. *J. Geophys. Res.* 95 (B7), 11,213–11,223.
- Kitamura, K., 2006. Constraint of lattice-preferred orientation (LPO) on Vp anisotropy of amphibole-rich rocks. *Geophys. J. Int.* 165, 1058–1065.
- Lister, G.S., Snoke, A.W., 1984. S-C mylonites. *J. Struct. Geol.* 6, 617–638.
- Lloyd, G.E., Kendall, J.-M., 2005. Petrofabric derived seismic properties of a mylonitic quartz simple shear zone: implications for seismic reflection profiling. In: Harvey, P.K., Brewer, T., Pezard, P.A., Petrov, V.A. (Eds.), *Petrophysical Properties of Crystalline Rocks: Sp. Publ. Geol. Soc. Lond.*, vol. 240, pp. 75–94.
- Mahan, K., 2006. Retrograde mica in deep crustal granulites: Implications for crustal seismic anisotropy. *Geophys. Res. Lett.* 33, L24301. doi:10.1029/2006GL028130.
- Mainprice, D., 1990. An efficient Fortran program to calculate seismic anisotropy from the lattice preferred orientation of minerals. *Comput. Geosci.* 16, 385–393.
- Mainprice, D., 2007. In: Schubert, G. (Ed.), *Seismic anisotropy of the deep Earth from a mineral and rock physics perspective*. Treatise in Geophysics, vol. 2. Elsevier, Oxford, pp. 437–492.
- Mainprice, D., Nicolas, A., 1989. Development of shape and lattice preferred orientations – application to the seismic anisotropy of the lower crust. *Journal of Structural Geology* 11, 175–189.
- Mainprice, D., Humbert, M., 1994. Methods of calculating petrophysical properties from lattice preferred orientation data. *Surv. Geophys.* 15, 575–592.
- Mainprice, D., Silver, P., 1993. Constraints on the interpretation of teleseismic SKS observations from kimberlite nodules from the subcontinental mantle. *Phys. Earth Planet. Inter.* 78, 257–280.
- McSkimin, H.J., Andreatch Jr., P., Thurston, R.N., 1965. Elastic moduli of quartz versus hydrostatic pressure at 25 °C and –195.8 °C. *J. Appl. Phys.* 36, 1624–1632.
- Meissner, R., Mooney, W.D., Artemieva, I., 2002. Seismic anisotropy and mantle creep in young orogens. *Geophys. J. Int.* 149, 1–14.
- Meissner, R., Rabbel, W., Kern, H., 2006. Seismic lamination and anisotropy of the lower continental crust. *Tectonophysics* 416, 81–99.
- Meltzer, A., Christensen, N., 2001. Nanga Parbat crustal anisotropy: implications for interpretation of crustal velocity structure and shear-wave splitting. *Geophys. Res. Lett.* 28 (28), 2129–2132.
- Nishizawa, O., Yoshino, T., 2001. Seismic velocity anisotropy in mica rich rocks: an inclusion model. *Geophys. J. Int.* 145, 19–32.
- Okaya, D.A., Christensen, N.I., 2002. Anisotropic effects of non-axial seismic wave propagation in foliated crustal rocks. *Geophys. Res. Lett.* 29. doi:10.1029/2001GL014285.
- Ozacar, A.A., Zandt, G., 2004. Crustal seismic anisotropy in central Tibet: implications for deformation style and flow in the crust. *Geophys. Res. Lett.* 31, L23601. doi:10.1029/2004GL021096.
- Readman, P.W., Hauser, F., O'Reilly, B.M., Do, V.C., 2009. Crustal anisotropy in southwest Ireland from analysis of controlled source shear-wave data. *Tectonophysics* 474, 571–583.
- Rudnick, R.L., Fountain, D.M., 1995. Nature and composition of the continental crust – a lower crustal perspective. *Rev. Geophys.* 33, 267–309.
- Savage, M.K., 1999. Seismic anisotropy and mantle deformation: what have we learned from shear wave splitting? *Rev. Geophys.* 37, 65–106.
- Schulte-Pelkum, V., Monsalve, G., Sheehan, A., Pandey, M.R., Sapkota, S., Bilham, R., Wu, F., 2005. Imaging the Indian subcontinent beneath the Himalaya. *Nature* 435, 1222–1225.
- Shapiro, N.M., Ritzwoller, M.H., Molnar, P., Levin, V., 2004. Thinning and flow of Tibetan crust constrained by seismic anisotropy. *Science* 305, 233.
- Sherrington, H.F., Zandt, G., Fredriksen, A., 2004. Crustal fabric in the Tibetan Plateau based on waveform inversions for seismic anisotropy parameters. *J. Geophys. Res.* 109, B02312. doi:10.1029/2002JB002345.
- Silver, P.G., 1996. Seismic anisotropy beneath the continents: probing the depths of geology. *Annu. Rev. Earth Planet. Sci.* 24, 385–432.
- Tatham, D.J., Lloyd, G.E., Butler, R.W.H., Casey, M., 2008. Amphibole and lower crustal seismic properties. *Earth Planet. Sci. Lett.* 267, 118–128.
- Valcke, S.L.A., Casey, M., Lloyd, G.E., Kendall, J.-M., Fisher, Q.J., 2006. Lattice preferred orientation and seismic anisotropy in sedimentary rocks. *Geophys. J. Int.* 166, 652–666.
- Vaughan, M.T., Guggenheim, S., 1986. Elasticity of muscovite and its relationship to crystal structure. *J. Geophys. Res.* 91, 4657–4664.
- Vergne, J., Wittlinger, G., Farra, V., Su, H., 2003. Evidence for upper crustal anisotropy in the Songpan-Ganze (northeastern Tibet) terrane. *Geophys. Res. Lett.* 30 (6–1), 4.
- Weiss, T., Siegesmund, S., Rabbel, W., Bohlen, T., Pohl, M., 1999. Seismic velocities and anisotropy of the lower continental crust: a review. *Pure Appl. Geophys.* 156, 97–122.
- Wendt, A.S., Bayuk, I.O., Covey-Crump, S.J., Wirth, R., Lloyd, G.E., 2003. An experimental and numerical study of the microstructural parameters contributing to the seismic anisotropy of rocks. *J. Geophys. Res.* 108 (B8), 2365. doi:10.1029/2002JB001915.
- Xu, L.L., Rondenay, S., van der Hilst, R.D., 2007. Structure of the crust beneath the southeastern Tibetan Plateau from teleseismic receiver functions. *Phys. Earth Planet. Inter.* 165, 176–193.
- Zeitler, P.K., Chamberlain, C.P., Smith, H.A., 1993. Synchronous anatexis, metamorphism, and rapid denudation at Nanga Parbat, Pakistan Himalaya. *Geology* 21, 347–350.
- Zeitler, P.K., Meltzer, A.S., Koons, P.O., Craw, D., Hallet, B., Chamberlain, C.P., Kidd, W.S., Park, S.K., Seeber, L., Bishop, M., Shroder, J., 2001. Erosion, Himalayan geodynamics and the geomorphology of metamorphism. *GSA Today* 11, 4–8.